The First Precision Photometric Observations and Analyses of the Totally Eclipsing, Solar Type Binary, V1302 Herculis

Ronald G. Samec
Pisgah Astronomical Research Institute, 318 Monti Drive, Anderson, SC 29625; ronaldsamec@gmail.com

Daniel Caton
Dark Sky Observatory, Department of Physics and Astronomy, Appalachian State University, 525 Rivers Street, Boone, NC 28608-2106; catondb@appstate.edu

Danny Faulkner
Johnson Observatory, 1414 Bur Oak Court, Hebron, KY 41048; dfaulkner@answersingenesis.org

Received August 26, 2022; revised May 2, 10, 2023; accepted May 10, 2023

Abstract CCD, BVRI light curves of the W UMa variable V1302 Her were taken on 24, May, 07, and 23. 24, 27 June 2020 at the Dark Sky Observatory, North Carolina, USA, with the 0.81-m reflector of Appalachian State University. From our present observations, which include three primary eclipses and three secondary eclipses, we determined a linear and a quadratic ephemeris:

JD Hel MinI = 2459027.6675±0.0033 + 0.3162911±0.0000003 × E

JD Hel MinI = 2459027.6764±0.0033d + 0.31629542±0.00000087 × E +

0.00000000027±0.00000000005 × E2

From our 16-year period study, the period is found to be increasing. This could be due to mass transfer making the mass ratio decrease (q = M2 / M1; all pairs of values should be corrected with a phase shift of 0.5). A Wilson-Devinney analysis reveals that the system is an A-type (more massive component is the hottest) overcontact W UMa binary with a fairly extreme mass ratio (q = 0.2426 ± 0.0003, 1 / q = M1 / M2 = 4.1). Its Roche Lobe fill-out is ~23%. One hot spot was needed in the solution. The temperature difference of the components is only ~263 K, with the more massive component as the slightly hotter one, so that in the present observations, it is an A-type W UMa binary. The inclination is high, 87.0 ± 0.2, resulting in a total primary eclipse.

1. History and observations

The variability of V1302 Her (GSC 3101-0683, 1SWASP J175239.07+434931.5) was detected in the FOV of the Algol-type binary V338 Her by the ROTSE1 experiment (Akerlof *et al.* 2000; ROTSE1 J175239.04+434936.7, Liakos and Niarchos 2009, see Figure 1.). They classified it as a contact variable with an ephemeris of HJD Min I = 2454610.3476169 + 0.3162897 d * E (Pejcha 2005). A nearby X-ray source, 1RXS J175245.6+435128, is likely associated with this star (Pejcha 2006). It is classified as a contact variable with a maximum V magnitude of 12.33 and amplitude of V ~ 0.4.

The system was observed by the All Sky Automated Survey as ASASSN-V J051858.09+365806.2 (Shappee *et al.* 2014; Kochanek *et al.* 2017), see Figure 2.). They give a V_{mean} = 11.33, an amplitude of 0.4, and EW designation, J–K = 0.467. The initial report was given in American Astronomical Society meeting #238 (Canton *et al.* 2021). Their ephemeris is:

$$\text{HJD Min I} = 2457070.80679 + 0.3995827\text{E d} \times \text{E} \quad (1)$$

From the ASAS-SN curves we were able to phase the data with Equation 1 and do parabola fits to the primary and secondary minima to locate two times of minimum within 0.001 phase of each minimum. We also included the ASAS-SN HJD Min I in our period study.

This system was observed as a part of our professional collaborative studies of interacting binaries at Pisgah Astronomical Research Institute from data taken from DSO observations.

The observations were taken by D. Caton, R. Samec, and D. Faulkner. Reduction and analyses were done by Ron Samec.

Our 2017 BVRI light curves were taken at Dark Sky Observatory, on 24, May, 07, and 23. 24, 27 June 2020 with a thermoelectrically cooled (–35° C) 1KX1K FLI camera and Bessell BVRI filters.

These observations consisted of 680 measurements in B, 707 in V, 717 in R, and 707 in I. The listed magnitudes are delta magnitudes in V–C. HJD are Heliocentric Julian dates. The probable error of a single observation was 4 mmag in B, V, and R, and 3 mmag in I. The nightly C–K values stayed constant throughout the observing run with a precision of about 1%. Exposure times varied from 45 s in B and 20 s in V to 15 s in R and I. To produce these images, nightly images were calibrated with 25 bias frames, at least five flat frames in each filter, and ten 300-second dark frames. Table 1 gives the BVRI observations.

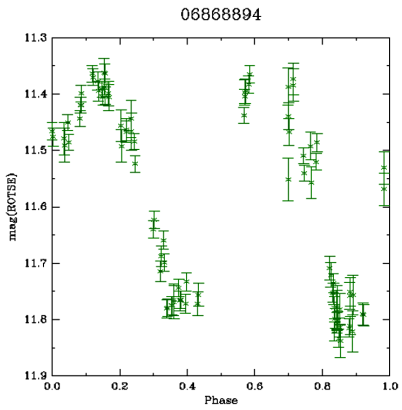

Figure 1. ROTSE light curves (Geske *et al.* 2006).

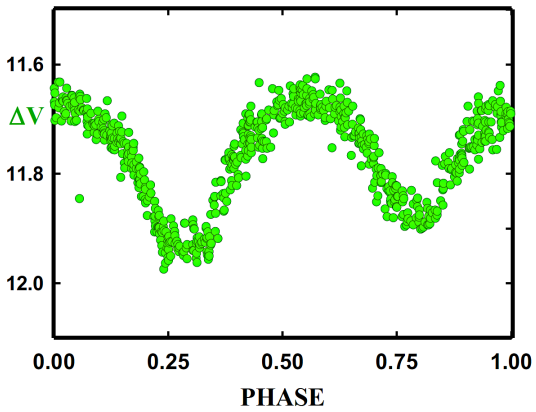

Figure 2. ASAS-SN data light curves (Shappee *et al.* 2014; Kochanek *et al.* 2017).

Table 1. Sample of first ten *V1302 Her B, V, R, I* observations.

ΔB (V–C)	*HJD 2458900+*	*ΔV (V–C)*	*HJD 2458900+*	*ΔR (V–C)*	*HJD 2458900+*	*ΔI (V–C)*	*HJD 2458900+*
2.619	93.8085	2.747	93.8064	2.742	93.8042	2.781	93.8044
2.619	93.8105	2.743	93.8076	2.764	93.8054	2.788	93.8056
2.626	93.8125	2.751	93.8089	2.753	93.8066	2.795	93.8069
2.621	93.8140	2.754	93.8110	2.753	93.8079	2.799	93.8081
2.619	93.8155	2.755	93.8130	2.758	93.8099	2.803	93.8101
2.621	93.8170	2.756	93.8145	2.766	93.8117	2.803	93.8120
2.620	93.8186	2.762	93.8161	2.763	93.8133	2.804	93.8135
2.617	93.8201	2.755	93.8176	2.743	93.8148	2.794	93.8150
2.608	93.8216	2.762	93.8191	2.767	93.8163	2.795	93.8166
2.610	93.8232	2.754	93.8206	2.768	93.8179	2.807	93.8181

Note: First ten data points of V1302 Her B, V, R, I observations. The complete table is available through the AAVSO ftp site at ftp://ftp.aavso.org/public/datasets/3851-Samec-511-v1302her.txt (if necessary, copy and paste link into the address bar of a web browser).

Table 2. The photometric target data.

Star	*Name*	*R.A. (2000) h m s*	*Dec. (2000) ° ′ ″*	*V*	*J–K*
V1302 Her	GSC 03101 0683 2MASS J17523906+4349293 UCAC3 268-144343 UCAC4 670-064717 Gaia DR2 1346420948207784704	17 52 39.0640592463[3]	+43 09 29.337600715[1]	11.373	0.469 ± 0.0333
C (comparison)	GSC 03101 1257	17 52 52.8323207873[4]	+43 50 48.212826632[4]	10.12 (0.03)	0.501 ± 0.047
K (check)	GSC 03101 0995	17 53 06.0206513889[4]	+43 52 6.243839274	9.752	0.246 ± 0.033

[1] *ICRS (IAU 2013).* [2] *2MASS (Skrutskie* et al. *2006).* [3] *UCAC3 (U.S. Naval Observatory 2012).* [4] *UCAC3 (Zacharias, N.,* et al. *2010).*

2. Photometric targets

The photometric targets (variable, comparison (C), and check (K) stars) of this paper are noted in Table 2. The finding chart with variable (V), comparison, and check stars is shown in Figure 3.

3. Period determination

Seven mean times of minimum light were calculated from our present observations (BVRI data), which included four primary and three secondary eclipses:

HJD I = 2458993.81742 ± 0.00106, 2459024.81490 ± 00007, 2459023.86008 ± 0.00056, 2459027.66111 ± 0.000128

HJD II = 2459024.65805 ± 0.00031, 2459023.71008 ± 0 0.00052, 2459027.82066 ± 0.00025.

These minima were weighted as 1.0 in the period study.

In addition, eight times of low light were calculated from ASAS-SN data and were weighted 0.1. Twenty times of minimum were taken from IBVS (Hübscher *et al.* 2010, 2012; Liakos and Niachos 2009; Pejcha 2005, 2006; Nelson 2015, 2017). This gave us a period study with an interval of ~16 years.

From these timings, two ephemerides have been calculated, a linear and a quadratic one:

$$\text{JD Hel Min I} = 2459027.65873 \pm 0.00080\,\text{d} + 0.31629036 \pm 0.00000072 \times \text{E} \quad (2)$$

$$\text{JD Hel Min I} = 2459027.66132 \pm 0.00054\,\text{d} + 0.31629221 \pm 0.00000017 \times \text{E} + 0.000000000121 \pm 0.000000000011 \times \text{E}^2 \quad (3)$$

The plotted residuals of the quadratic term are given in Figure 4. The errors are too small to be given in the figure or are nonexistent (from visual timings or times of single ASAS-SN observations, usually within 0.001s of the fitted minima). These are used in the absence of enough observed minima to do a period study. They have been found to work well in this situation.).

The study given here covers a time interval of 16 years. It does show an orbital period that is increasing, as shown in the O–C curve. This might be due to mass transfer to the more massive, primary component making the mass ratio more extreme.

The quadratic ephemeris yields a $\dot{P} = 1.7(0.5) \times 10^{-7}\,\text{d/yr}$ or a mass exchange rate of

$$dM/dt = (\dot{P} M_1 M_2)/(3P(M_1 - M_2)) = 8(3) \times 10^{-8} M_\odot/\text{yr}$$

in a conservative scenario (the primary component is the gainer; see van der Sluys 2021). The O–C table of minima with linear and quadratic residuals is shown in Table 3. The initial ephemeris for the table and to begin the calculation was

$$\text{JD Hel Min I} = 2459027.661109 + 0.3162897000 \times \text{E}.$$

4. Light curve characteristics

The curves are of good accuracy, averaging about 2% photometric precision. The amplitude of the light curve varies from 0.506 to 0.581 mag for I to B. The O'Connell effect, an indicator of spot activity, was 0.017–0.040 mag, B to I, indicating that magnetic activity is likely. The difference in minima, 0.062 to 0.046 B to I, indicates overcontact light curves in poor thermal contact. A total eclipse occurs at our secondary minima and lasts some 34 minutes. Complete light curve characteristics are given in Table 4.

5. Light curve solution

The 2MASS, J–K = 0.469 ± 0.033 for the binary star. These correspond to ~K0.5V ± 2.5, which yields a temperature of 5250 ± 200 K. Fast rotating binary stars of this type are noted for having strong magnetic activity, so the binary is of solar type with a convective atmosphere.

The B, V, R, and I curves were pre-modeled with Binary Maker 3.0 (Bradstreet and Steelman 2002). Fits were determined in all four filter bands and like parameters (like inclination) were averaged. The solution was that of an overcontact eclipsing binary. The parameters were then averaged (q = 0.21, fill-out = 0.0875, i = 86°, T_1 = 4950, with one 15° cool spot, T-FACT = 0.7) and input into a four-color simultaneous light curve calculation using the Wilson-Devinney Program (Wilson and Devinney 1971; Wilson 1990, 1994; van Hamme and Wilson 1998). A solution is arrived at when all parameter corrections are smaller than their associated standard deviations for each parameter. The solution was computed in Mode 3 and converged to a solution. In the case of the Wilson program (a differential corrections routine) this means that the corrections to the parameters are made at each iteration until they are smaller than their standard deviations. Convective parameters, g = 0.32, A = 0.5 were used. An eclipse duration of ~34 minutes was determined for our secondary eclipse and the light curve solution. The more massive component is the coolest one, making the system a W-type W UMa contact binary. We tried third light but that did not solve any fitting issues. The spotted solution follows in Table 5. At the request of the referee a non-spotted was undertaken. This solution is also given in Table 5. The goodness of fit parameter, Sum(W*Res**2), shows that the spotted solution is considerably better.

The BV and RI solution plots are given in Figures 5 and 6. The geometric surface (Roche Lobes) at quadratures is shown

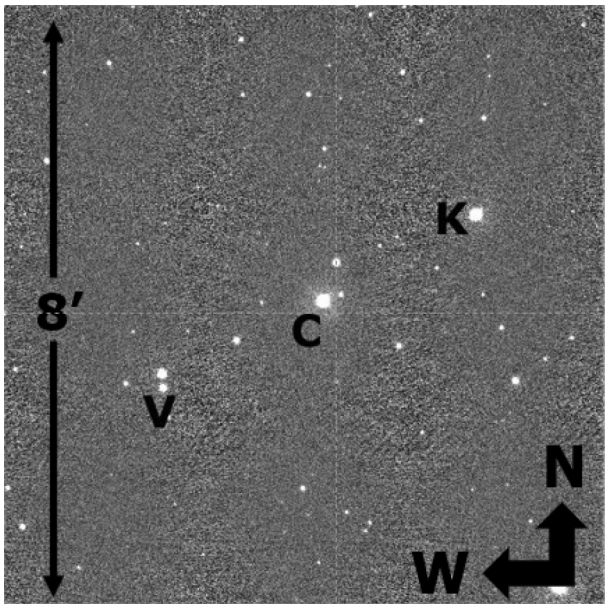

Figure 3. The finding chart for V1302 Her with variable (V), comparison (C), and check stars (K).

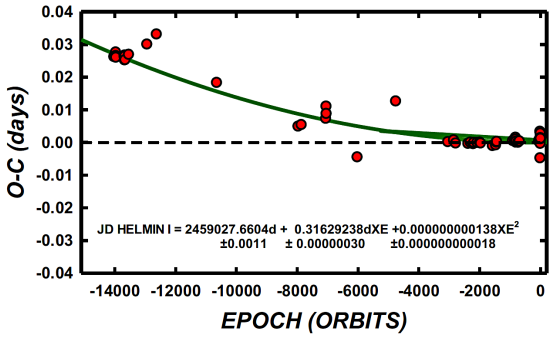

Figure 4. The plotted residuals of the quadratic term. Errors are smaller than the point size for regular minima (not times of low light).

Table 3. O–C residuals of minima, V1302 Her.

	Epoch (JD–2400000.0000)	*Cycle*	*Initial Res.*	*Linear Res.*	*Quad. Res.*	*Wt.*	*Reference*
1	53258.3739 ± 0.0008	18240.5	–0.0049	0.0095	0.0004	1.0	Pejcha (2005)
2	54591.5278 ± 0.0001	14025.5	–0.0121	–0.0004	–0.0009	1.0	Hübscher *et al.* (2010)
3	54609.3997 ± 0.0002	13969.0	–0.0106	0.0011	0.0007	1.0	Liakos and Niarchos (2009)
4	54610.3475 ± 0.0001	13966.0	–0.0117	0.0000	–0.0004	1.0	Liakos and Niarchos (2009)
5	54610.5055 ± 0.0002	13965.5	–0.0118	–0.0002	–0.0005	1.0	Liakos and Niarchos (2009)
6	54611.4540 ± 0.0002	13962.5	–0.0122	–0.0005	–0.0009	1.0	Liakos and Niarchos (2009)
7	54699.3835 ± 0.0003	13684.5	–0.0112	0.0002	0.0003	1.0	Liakos and Niarchos (2009)
8	54700.3326 ± 0.0003	13681.5	–0.0110	0.0005	0.0005	1.0	Liakos and Niarchos (2009)
9	54701.2817 ± 0.0004	13678.5	–0.0107	0.0007	0.0008	1.0	Liakos and Niarchos (2009)
10	54701.4384 ± 0.0004	13678.0	–0.0122	–0.0007	–0.0007	1.0	Liakos and Niarchos (2009)
11	54703.3363 ± 0.0003	13672.0	–0.0120	–0.0006	–0.0005	1.0	Liakos and Niarchos (2009)
12	54704.4433 ± 0.0006	13668.5	–0.0120	–0.0006	–0.0005	1.0	Liakos and Niarchos (2009)
13	54706.3421 ± 0.0003	13662.5	–0.0110	0.0005	0.0005	1.0	Liakos and Niarchos (2009)
14	54707.4480 ± 0.0004	13659.0	–0.0121	–0.0007	–0.0006	1.0	Liakos and Niarchos (2009)
15	54744.2977 ± 0.0004	13542.5	–0.0101	0.0012	0.0015	1.0	Hübscher *et al.* (2010)
16	54934.5507[2]	12941.0	–0.0054	0.0056	0.0066	0.2	Nelson (2017)[1]
17	55659.4811 ± 0.0055	10649.0	–0.0110	–0.0016	0.0018	0.2	Nelson (2014, 2017)
18	56507.4476 ± 0.0008	–7968.0	–0.0172	–0.0095	–0.0051	1.0	Hübscher (2014)
19	56540.3425 ± 0.0008	–7864.0	–0.0164	–0.0088	–0.0043	0.5	Hübscher (2014)
20	56794.8016 ± 0.0005	–7059.5	–0.0124	–0.0053	–0.0009	1.0	Nelson (2015)
21	56799.3916 ± 0.0055	–7045.0	–0.0086	–0.0015	0.0029	1.0	Hübscher *et al.* (2015)
22	56799.5475 ± 0.0007	–7044.5	–0.0108	–0.0038	0.0007	1.0	Hübscher *et al.* (2015)
23	57183.9985[1]	–5829.0	–0.0099	–0.0037	0.0004	0.1	Shappee 2014
24	56757.9535[1]	–7176.0	–0.0127	–0.0056	–0.0011	0.1	Shappee 2014
25	56757.9538[1]	–7176.0	–0.0125	–0.0053	–0.0009	0.1	Shappee 2014
26	56857.9030[1]	–6860.0	–0.0107	–0.0038	0.0006	0.1	Shappee 2014
27	57296.7571[1]	–5472.5	–0.0086	–0.0026	0.0013	0.1	Shappee 2014
28	57048.1516[1]	–6258.5	–0.0104	–0.0039	0.0004	0.1	Shappee 2014
29	58027.7101[1]	–3161.5	–0.0012	0.0033	0.0054	0.1	Shappee 2014
30	56797.9671[1]	–7049.5	–0.0098	–0.0027	0.0017	0.1	Shappee 2014
31	57522.9120 ± 0.0010	–4757.5	–0.0009	0.0047	0.0081	0.5	Nelson (2014, 2017)
32	58993.8174 ± 0.0003	–107.0	–0.0007	0.0018	–0.0006	0.5	Present observations
33	59024.6581 ± 0.0001	–9.5	0.0017	0.0041	0.0015	1.0	Present observations
34	59024.8149 ± 0.0008	–9.0	0.0004	0.0028	0.0002	1.0	Present observations
35	59023.7101 ± 0.0008	–12.5	0.0026	0.0050	0.0024	1.0	Present observations
36	59023.8601 ± 0.0006	–12.0	–0.0056	–0.0032	–0.0057	1.0	Present observations
37	59027.6611 ± 0.0001	0.0	0.0000	0.0024	–0.0002	1.0	Present observations
38	59027.8207 ± 0.0003	0.5	0.0014	0.0038	0.0012	0.5	Present observations

[1] *Times of low light.* [2] *Visual.*

in Figures 7a, b, c, and d. The system dimensions are given in Table 6 and the estimated system absolute parameters are given in Table 7. These are based on the system radii from the Wilson program and the densities from Roche lobe calculations using the period input into Binary Maker 3.

6. Discussion

V1302 Her is a A-type, overcontact W UMa binary. Since the eclipses were total, the mass ratio, $q=0.24$ ($1/q=4.12$), is well determined with a fill-out of 23(1)%. The system has a fairly extreme mass ratio and a component temperature difference of ~263 K, so it is in good thermal contact. One spot was needed in the final modeling. The inclination of ~87° resulted in a total eclipse in the secondary ($p_{shift}=0.5$, from the binary maker hand fit). Its photometric spectral type indicates a surface temperature of ~5250 K for the primary1 component, making it a solar type binary. Such a main sequence star would have a mass of ~0.86 $M_\odot$ (K0.5V) and the secondary (from the mass ratio) would have a mass of ~0.21 $M_\odot$ (making it very much undersized). The temperature of the primary component (~5513 K) of a main sequence star would make it of type G7V instead of M5V as indicated by its mass. This is probably due to substantial magnetic (dark spots) activity causing the more massive component to have a suppressed surface temperature. The period of this binary indicates that it is increasing. This could be due to mass exchange with the flow toward the more massive component making the mass ratio more extreme ($dM/dt=+8.11\times10^{-8} M_\odot/s$).

Radial velocity curves are needed to obtain absolute (not relative or estimated) system parameters.

Table 4. Light curve means and differences at quadratures, V1302 Her.

Filter	*Phase Mag Min I*	*Phase Mag Max I*
	0.00	0.25
B	2.644 ± 0.021	2.063 ± 0.025
V	2.775 ± 0.013	2.215 ± 0.017
R	2.761 ± 0.081	2.248 ± 0.021
I	2.799 ± 0.020	2.293 ± 0.022
Filter	*Phase Mag Min II*	*Phase Mag Max II*
	0.50	0.75
B	2.582 ± 0.016	2.080 ± 0.025
V	2.712 ± 0.018	2.247 ± 0.017
R	2.729 ± 0.011	2.290 ± 0.021
I	2.753 ± 0.020	2.333 ± 0.022

Filter	*Min I–Max I*	*Max II–MaxI*	*Min –Min II*
B	0.581 ± 0.046	0.017 ± 0.017	0.062 ± 0.037
V	0.560 ± 0.030	0.032 ± 0.032	0.063 ± 0.032
R	0.513 ± 0.102	0.042 ± 0.042	0.032 ± 0.092
I	0.506 ± 0.043	0.040 ± 0.040	0.046 ± 0.040
Filter	*Min II–Max I*	*Min I–Max II*	*Min II–Max II*
B	0.519 ± 0.041	0.564 ± 0.046	0.502 ± 0.041
V	0.497 ± 0.035	0.528 ± 0.030	0.465 ± 0.035
R	0.481 ± 0.032	0.471 ± 0.102	0.439 ± 0.032
I	0.460 ± 0.042	0.466 ± 0.043	0.420 ± 0.042

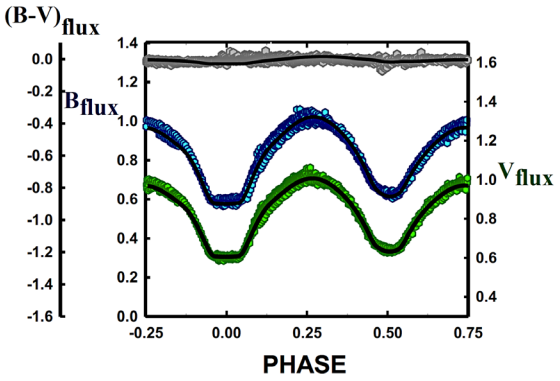

Figure 5. B,V light curve solution overlying the normalized flux curves. B is in blue and V in green. Gray is B–V.

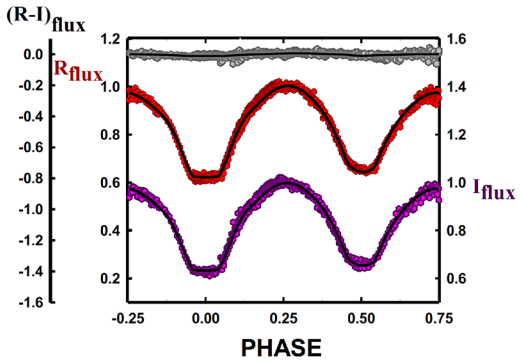

Figure 6. R,I light curve solution underlying the normalized flux curves. R is in red and I in purple. Gray is R-I.

Table 5. Light curve solutions of V1302 Her.

	Parameters	*Spotted Solution*	*Unspotted Solution*
	λ_B, λ_V, λ_R, λ_I (nm)	440, 550, 640, 790	440, 550, 640, 790
	g_1, g_2	0.32	0.32
	A_1, A_2	0.5	0.5
	Inclination (°)	87.0 ± 0.2	85.3 ± 0.3
	T_1, T_2 (K)1	5250, 5513 ± 2	5250, 5607 ± 2
	$\Omega_1 = \Omega_2$	2.301 ± 0.001	2.301 ± 0.002
	$q(m_1/m_2)$[1]	0.2426 ± 0.0003	0.2422 ± 0.0003
	Fill-outs: F1, F2 (%)	23.0 ± 0.51	22 ± 11
	$L_1/(L_1+L_2)_I$	0.7480 ± 0.0005	0.7379 ± 0.0006
	$L_1/(L_1+L_2)_R$	0.7427 ± 0.0005	0.7307 ± 0.0006
	$L_1/(L_1+L_2)_V$	0.7350 ± 0.0006	0.7202 ± 0.0007
	$L_1/(L_1+L_2)_V$	0.7194 ± 0.0008	0.6985 ± 0.0009
	JD_o (days)	2459027.66191 ± 0.00006	2459027.66281 ± 0.00007
	Period (days)	0.3163106 ± 0. 0000015	0.3163083 ± 0.0000018
	P-shift$_2$	0.5 added to phase	0.5
	Dimensions		
	$r_1/a, r_2/a$ (pole)	0.480 ± 0.001, 0.255 ± 0.002	0.480 ± 0.001, 0.254 ± 0.002
	$r_1/a, r_2/a$ (side)	0.522 ± 0.002, 0.266 ± 0.003	0.521 ± 0.001, 0.265 ± 0.002
	$r_1/a, r_2/a$ (back)	0.548 ± 0.002, 0.307 ± 0.006	0.548 ± 0.002, 0.305 ± 0.004
	Spot I, Primary Component	*Polar Hot Spot Region*	
	Colatitude (°)	32.19 ± 0.26	
	Longitude (°)	59 ± 1	
	Radius (°)	19.4 ± 0.1	
	T-Factor	1.195 ± 0.003	
	[3]Sum(W*Res**2)	0.774315	1.193995

[1] The errors are given by the Wilson code. Fill-out errors are determined from the combined errors of possible mass ratios and potentials (referee's note: these are underestimated). [2] The P-Shift = 0.5 means that in the normal sense (for ease in modeling), all primaries are replaced by secondaries and vv., (1↔2). [3] Goodness of fit parameter N.

Table 6. Estimates of V1302 Her system dimensions.

R_1, R_2 (pole, $R_\odot$)	0.961 ± 0.002	0.509 ± 0.005
R_1, R_2 (side, $R_\odot$)	1.044 ± 0.003	0.532 ± 0.006
R_1, R_2 (back, $R_\odot$)	1.097 ± 0.004	0.613 ± 0.012

Table 7. Estimated absolute parameters.[1]

Parameter	*Star 1*	*Star2*
Mean Radius ($R_\odot$)	1.003	0.552
Mean density	1.111 ± 0.004	1.803 ± 0.006
Mass ($M_\odot$)	0.87	0.21
Log g	4.34	4.29

[1] *Using light curve solution units, a = 1, a is calculated for Wilson program, and the semi-major axis. The density is in g/cm³ a = 2.00 $R_\odot$ (Binary Maker, Bradstreet and Steelman 2002).*

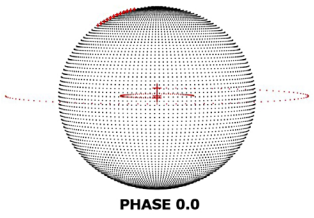

Figure 7a. Geometrical representation at phase 0.0

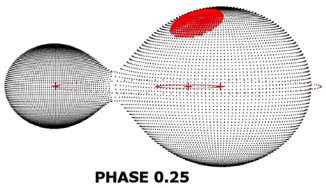

Figure 7b. Geometrical representation at phase 0.25.

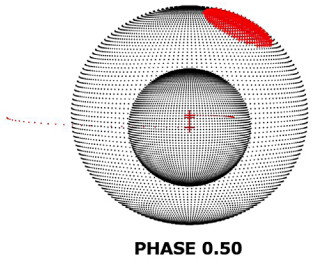

Figure 7c. Geometrical representation at phase 0.50.

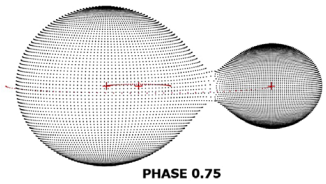

Figure 7d. Geometrical representation at phase 0.75.

References

Akerlof, C. *et al.* 2000, *Astron. J.*, **119**, 1901.

Bradstreet, D. H., and Steelman, D.P. 2002, *Bull. Amer. Astron. Soc.*, **34**, 1224.

Caton, D. B., Samec, R., and Faulkner, D. 2021, *Bull. Amer. Astron. Soc.*, **53**, e-id 2021n6i215p05.

Geske, M. T., Gettel, S. J., and McKay, T. A. 2006, *Astron. J.*, **131**, 633.

Hübscher, J. 2014, *Inf. Bull. Var. Stars*, No. 6118, 1.

Hübscher, J., and Lehmann, P. B. 2015, *Inf. Bull. Var. Stars*, No. 6149, 1.

Hübscher, J., Lehmann, P. B., Monninger, G., Steinbach, H.-M. and Walter, F. 2010, *Inf. Bull. Var. Stars*, No. 5918, 1.

Hübscher, J., Lehmann, P. B., and Walter, F. 2012, *Inf. Bull. Var. Stars*, No. 6010, 1.

International Astronomical Union. 2013, International Earth Rotation and Reference Systems Service, International Celestial Reference System (ICRS; https://www.iers.org/IERS/EN/Science/ICRS/ICRS.html).

Kochanek, C. S., *et al.* 2017, *Publ. Astron. Soc. Pacific*, **129**, 104502.

Liakos, A., and Niarchos, P. 2009, *Inf. Bull. Var. Stars*, No. 5897, 1.

Nelson, R. H. 2014, AAVSO O–C database (https://www.aavso.org/bob-nelsons-o-c-files).

Nelson, R. H. 2015, *Inf. Bull. Var. Stars*, No. 6131, 1.

Nelson, R. H. 2017, *Inf. Bull. Var. Stars*, No. 6195, 1.

Pejcha, O. 2005, *Inf. Bull. Var. Stars*, No. 5645, 1.

Pejcha, O. 2006, *Inf. Bull. Var. Stars*, No. 5699, 15.

Shappee, B. J., *et al.* 2014, *Astrophys. J.*, **788**, 48.

Skrutskie, M. F., *et al*. 2006, "The Two Micron All Sky Survey," *Astron. J.*, **131**, 1163.

U.S. Naval Observatory. 2012, UCAC-3 (http://www.usno.navy.mil/USNO/astrometry/optical-IR-prod/ucac).

van der Sluys, M. 2021, "Binary evolution in a nutshell (BEiaNS)."[1]

van Hamme, W. V., and Wilson, R. E. 1998, *Bull. Amer. Astron. Soc.*, **30**, 1402.

Wilson, R. E. 1990, *Astrophys. J.*, **356**, 613.

Wilson, R. E. 1994, *Publ. Astron. Soc. Pacific*, **106**, 921.

Wilson, R. E., and Devinney, E. J. 1971, *Astrophys. J.*, **166**, 605.

Zacharias, N., *et al.* 2010, *Astron. J.*, **139**, 2184.

[1] van der Sluys (2021), "Binary evolution in a nutshell (BEiaNS)" (https://astro.ru.nl/~sluys/Binaries/files/BinaryEvolutionNutshell_letter.pdf).